

Entropy can bundle nanowires in good solvents

Hongyu Gao,[†] Simon Bettscheider,^{‡,¶} Tobias Kraus,^{‡,¶} and Martin H. Müser^{*,†}

[†]*Department of Materials Science and Engineering, Saarland University, Campus C6 3,
66123 Saarbrücken, Germany*

[‡]*INM - Leibniz Institute for New Materials, Campus D2 2, 66123 Saarbrücken, Germany*

[¶]*Colloid and Interface Chemistry, Saarland University, Campus D2 2, 66123 Saarbrücken,
Germany*

E-mail: martin.mueser@mx.uni-saarland.de

Phone: +49 681 302 57452. Fax: +49 681 302 57454

Abstract

Surfaces with surface-bound ligand molecules generally attract each other when immersed in poor solvents but repel each other in good solvents. While this common wisdom holds, for example, for oleylamine-ligated ultrathin nanowires in the poor solvent ethanol, the same nanowires were recently observed experimentally to bundle even when immersed in the good solvent *n*-hexane. To elucidate the respective binding mechanisms, we simulate both systems using molecular dynamics. In the case of ethanol, the solvent is completely depleted at the interface between two ligand shells so that their binding occurs, as expected, via direct interactions between ligands. In the case of *n*-hexane, ligands attached to different nanowires do not touch. The binding occurs because solvent molecules penetrating the shells preferentially orient their backbone normal to the wire, whereby they lose entropy. This entropy does not have to be summoned a second time when the molecules penetrate another nanowire. For the

mechanism to be effective, the ligand density must be intermediate, i.e., small enough to allow solvent molecules to penetrate, but not so small that ligands do not possess a clear preferred orientation at the interface to the solvent. At the same time, solvent molecules may be neither too large nor too small for similar reasons. Experiments complementing the simulations confirm the predicted trends.

1 Introduction

Ultrathin gold nanowires (AuNWs) are chemically synthesized particles that exist as colloidal dispersions in apolar solvents.¹⁻³ They consist of a metal gold core with a diameter as small as 1.7 nm, which is surrounded by a shell of oleylamine molecules of similar thickness. The nanowires form when gold chloride salts are reduced in the presence of oleylamine. Their length depends on reaction time; values of up to 6.4 μm have been reported.⁴ The large aspect ratio of the wires above 10^3 and their limited bending stiffness lead to an unusual type of agglomeration: the wires can spontaneously self-assemble into bundles. This was first observed in the original synthesis of AuNWs^{5,6} and studied in more detail by Loubat et al.⁷ The bundles that formed in the presence of excess oleylamine from synthesis exhibited a hexagonal arrangement of 10 to 100 parallel AuNWs that were separated by two double layers of oleylamine at a wire-wire distance of 9.7 nm.

Nanowire bundling has interesting technological implications. For example, Liz-Marzan and co-workers used the formation of AuNW networks to create disordered, conductive meshes at a gas-liquid interfaces, which they deemed suitable as transparent conductive electrodes.⁸ Maurer et al. used an elastomer stamp to direct the bundling wires into regular meshes, which were applicable for touch-screen devices,^{9,10} while Gong et al. casted electrode patterns of nanowire bundles onto a glove to create a wearable strain sensor.¹¹ It is even possible to extrude or “spin” the wires into macroscopic fibers with mechanical properties that depend on the degree of shear alignment.¹²

While much phenomenology is known about the bundling of nanowires, our present un-

derstanding of the bundling mechanism is rather limited. For example, Reiser et al.¹³ systematically altered the solvent and showed that purified AuNWs in *n*-hexane packed more densely (wire-wire distance of 5.5 nm) than as-synthesized AuNWs with only two sheets of oleylamine in between their gold core surfaces.¹³ Even tighter bundles were formed when AuNWs were dispersed in polar solvents such as ethanol¹² or when the ligand oleylamine was replaced by the shorter trioctylphosphine as demonstrated by Nouh et al.¹⁴ No ordered bundling was observed when purified AuNWs were redispersed in apolar cyclohexane.¹³

Little is known about the molecular origin of the exact spacing and its dependence on the solvent and its quality. Most importantly, it is not understood why AuNWs sometimes bundle in good solvents and sometimes do not. The shape of the wires apparently plays a role: spherical gold nanoparticles coated with oleylamine are stable against agglomeration in *n*-hexane even if the gold cores are as large as 12 nm.¹⁵⁻¹⁸ Reiser and co-authors suggested a “supramolecular” origin of bundling.¹³ Despite its appeal, this argument is somewhat vague.

The binding mechanism in our system of interest can certainly not be fully explained in terms of usually successful coarse-graining approaches casting the effect of good solvents as two-body repulsion between monomers.¹⁹ We believe that it belongs to the cases where an effective modeling of intricate solvent-induced phenomena requires the solvent to be treated explicitly. Examples include cononsolvency²⁰ and an almost perfectly suppressed interdigitation of solvated hydrophobic and solvated hydrophilic polymer brushes.²¹ We therefore run large-scale, explicit-solvent simulations of our system of interest. In order to acquire reliable potentials of mean force (per unit length) between two nanowires in good and poor solvents alike, the umbrella sampling strategy was adopted to our problem.

2 Methodology

Molecular dynamics (MD) simulations were carried out based on a representative model system shown in Fig. 1, where two identical AuNWs, each grafted with 62 ligand molecules

(oleylamine), were embedded in a *n*-hexane (or an ethanol) solvent. The central cylindrical Au wires with 0.85 nm radius and 3.01 nm length were treated as rigid bodies throughout the simulation, because bending, for example induced by thermal fluctuations, is negligible on the nanometer scale. Both NWs were oriented parallel to the *z*-axis, one was fixed in space, while the other one was free to move along the *x*- and *z*-axis as well as to rotate about its symmetry axis. To effectively deduce pair interactions between bundled AuNWs, only two NWs were included. While three-wire (and higher-order wire) interactions may slightly change the interactions between wires on a triangular lattice, significant many-body interactions require the soft shell to be small compared to the rigid core.²² Moreover, the simulations are already very demanding for dimers because of the used realistic all-atom force field. This is why it is scarcely feasible at this point to reliably compute the expectedly small many-wire corrections to construct accurate many-wire free-energy surfaces.

The ligands were randomly distributed on the Au wire surfaces with a mean grafting density of approximately 3.8 ligands/nm², which falls into the range of typical experimental values.^{23,24} When a new anchoring site was drawn, a constraint ensured that the new site had a distance of at least 0.47 nm to all preexisting anchoring atoms, so that nearest-neighbor Au atoms could not be simultaneously anchoring sites. Periodic boundary conditions were applied at the boundaries of the simulation domain (Fig. 1) in all three spatial directions. This way, the wires had neither beginning nor end. The size of the simulation cell was 24.6 nm in *x* and 9 nm in *y* direction. This geometry certainly provides a sufficiently large buffer to suppress any noticeable interaction between the wire pair and its periodic images, at least for the given maximum distance of the wires of $\Delta x_{\max} \approx 8$ nm.

A key assumption of our model is that the amine end of a ligand is connected to the Au surface by a strong permanent bond. Such an arrangement should not affect the results very much as long as bonds between the amine groups and the front gold atoms are sufficiently strong²⁵ so that the coverage density remains constant. Due to the lack of well-tested interatomic potentials between gold atoms and amine groups, and due to the close-packed

structure of gold atoms on the surface, we took the liberty of describing the bonds between them with the same set of parameters as between two methylene groups. This imposes no preferred bond angles on the gold atoms, but a tetrahedral bond angle on the amine group. As the ligands are relatively long, we do not expect it to be important to work with a more realistic bond angle on the amine group.

The wire-wire radial distribution function $g(r)$ — from which the potential of mean force $F(r)$ follows — was obtained by monitoring the thermal fluctuations of the interwire spacing after equilibration had occurred. This was done with umbrella sampling. Specifically, in order to acquire good statistics for all (relevant) distances, a harmonic biasing potential

$$V_{\text{bias}} = \frac{k}{2} (r - r_s)^2, \quad (1)$$

was applied, where k is the spring constant and r_s the distance between the center of masses of the two wires. The effect of the biasing spring was subtracted for the construction of the “real” two-body (free) energy through

$$F(r) = F_0(r_s) - k_B T \ln g(r, r_s) - V_{\text{bias}}(r, r_s), \quad (2)$$

where $F_0(r_s)$ is an offset, T is the temperature of the system, $g(r, r_s)$ the radial distribution function for the given value of r_s , and k_B the Boltzmann constant. For reasons of completeness, it shall be mentioned that the spring constant was finalized as $k = 0.07$ N/m after multiple attempts on its effectiveness. Moreover, six different equilibrium spring positions r_s were investigated, where adjacent ones were separated by 0.4 nm to 0.6 nm.

The temperature and pressure of the system were maintained at 330 K and 1 bar, respectively, using an isothermal-isobaric (NPT) ensemble with an integration timestep of 1 fs. The temperature was slightly (10%) higher than that in the experiment (i.e. room temperature) so as to achieve better sampling by reducing the viscosity of the solution. Since the ligands and both investigated solvents are far away from a phase transition, $F(r)$ can only depend

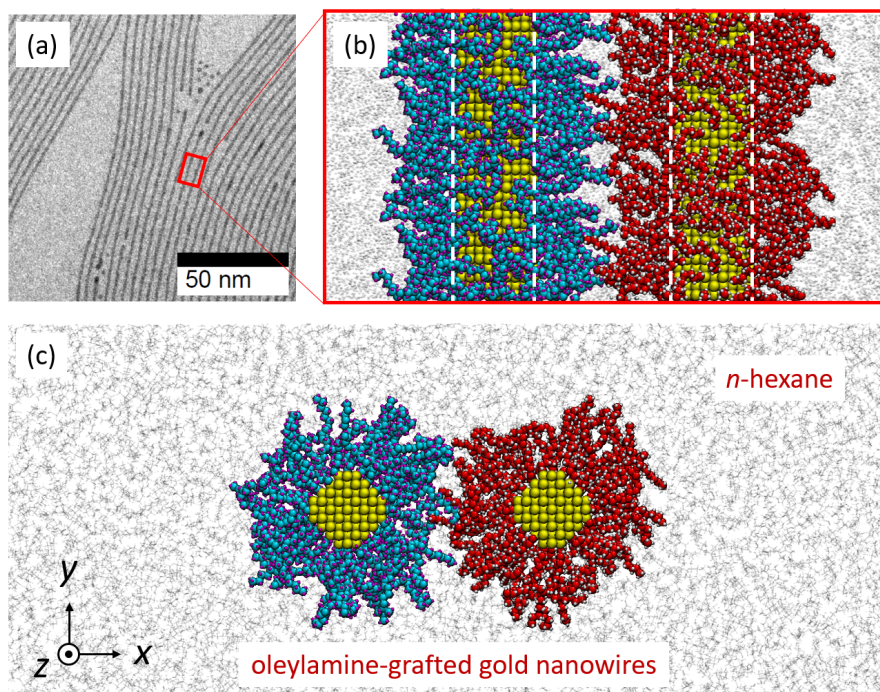


Figure 1: (a) TEM micrograph of bundled ultrathin gold nanowires. (b-c) Projections of representative MD configurations for near-equilibrium spacings onto (b) the xz -plane and (c) the xy -plane. n -hexane is the solvent in both cases. (Au: gold; oleylamine C/H: blue/purple on the left wire and red/white on the right wire; and n -hexane: gray). Periodic box dimensions are $l_x = 24.6$ nm, $l_y = 9.0$ nm, and $l_z = 3.3$ nm.

weakly on temperature. Thus, results for $F(r)$ at the laboratory temperature of $T \approx 300$ K must be similar to those at the simulation temperature of $T = 330$ K.

For each value of r_s , the system was found to have equilibrated within the first 1 ns simulation time. Each equilibration was followed by another 200 ns simulation, over which data was collected for post-processing. Interactions within the system were described using the all-atom OPLS force field.²⁶ The used parameters are provided in the *Supporting Information* (SI). All the simulations were carried out using the open-source MD code LAMMPS.²⁷

We evaluated the spacing of the wires experimentally using previously published method in order to verify the measured valued and to extend the range of solvents. Details can be found in the SI.

3 Results and discussion

3.1 Potential of mean force and interwire distance

Equilibrium MD simulations based on the model system shown in Fig. 1 were carried out at each given equilibrium spring length r_s . As discussed in Sec. 2.2, separate simulations with different r_s can be effective in exploring the phase space that is poorly sampled in thermal equilibrium. Averaging over 200 ns is sufficient to achieve reliable statistics for each value of r_s . A probability density distribution of dynamic interwire spacing, $\text{Pr}(r)$, can thus be determined as data points as shown in Fig. 2, with peaks close to r_s .

For each value of r_s , the normalized $\text{Pr}(r)$ was fitted with a skew normal distribution (SND) function,²⁸ defined by

$$\text{Pr}_{\text{SND}}(r, \sigma, \mu, \alpha) \equiv \frac{2}{\sigma} \cdot \phi\left(\frac{r - \mu}{\sigma}\right) \cdot \Phi\left[\frac{\alpha(r - \mu)}{\sigma}\right], \quad (3)$$

where $\phi(x) \equiv \exp(-x^2/2)/\sqrt{2\pi}$ is the standard Gaussian, $\Phi(x) \equiv [1 + \text{erf}(x/\sqrt{2})]/2$ its cumulative distribution function, and $\text{erf}(x/\sqrt{2})$ is the error function. α is a shape parameter,

which is greater (or less) than zero if the distribution is right (or left) skewed. SND suits better for our purpose than conventional Gaussians because the asymmetry (or skewness) of a distribution can be captured in leading order. Both the MD-derived $\text{Pr}(r)$ (data points) and the results from SND fitting (solid curves) are shown in Fig. 2 for *n*-hexane; the corresponding fitting parameters are listed in table 1. For a given value of r , the data set, for which the fit to $\text{Pr}(r, r_s)$ turned out largest, was selected to be the relevant data set at the value of r in the construction of the combined $F(r)$.

Table 1: Fitted SND parameters

	r_s (nm)					
hexane	4.7	5.1	5.5	5.9	6.4	7.0
μ (nm)	4.75	5.37	5.32	5.70	6.36	6.99
σ (nm)	0.21	0.28	0.32	0.32	0.26	0.27
α (—)	0.57	-1.58	2.05	1.26	0.10	0.13

	r_s (nm)			
ethanol	3.15	5.1	3.95	4.35
μ (nm)	3.15	3.41	3.73	4.02
σ (nm)	0.19	0.23	0.18	0.17
α (—)	1.79	2.74	1.53	1.37

Table 2: Fitted PMF parameters

	V_{rep} ($k_B\text{K}/\text{nm}$)	ρ_{rep} (nm)	V_{adh} ($k_B\text{K}/\text{nm}$)	r_{adh} (nm)	ρ_{adh} (nm)
hexane	$7.23 \cdot 10^6$	0.47	65.78	6.02	0.55
ethanol	$1.55 \cdot 10^6$	0.42	398.03	3.84	0.25

A potential of mean force (PMF) for the wire-wire separation was deduced from the various $\text{Pr}(r)$ according to Eq. (2). Note that, for reasons of simplicity, the abbreviation PMF is used, irrespective of whether or not the energy is normalized to length. The offsets $F_0(r_s)$ were chosen such that the combined $F(r)$ was a smooth function in r while obeying the boundary condition $F(r \rightarrow \infty) \rightarrow 0$. The ultimate PMF was obtained by fitting the

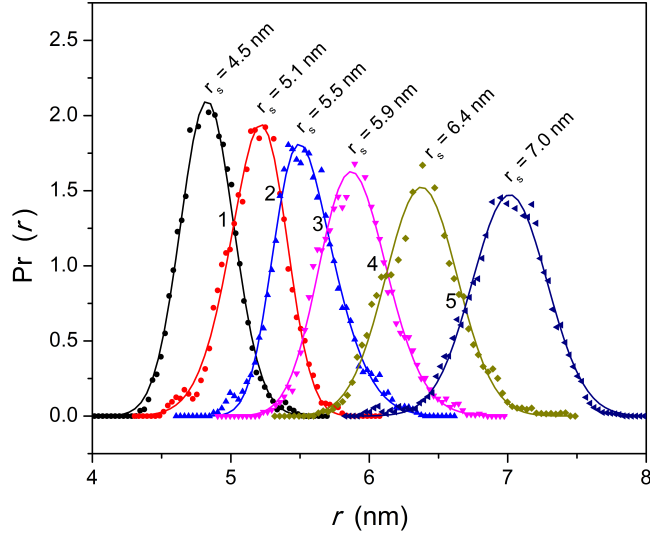


Figure 2: Probability densities of interwire distance in *n*-hexane for cases of varied spring equilibrium distances (differentiated by colors). MD results are shown with symbols, to which $\text{Pr}(r)$ (solid curves) were fitted with a skew normal distribution function.

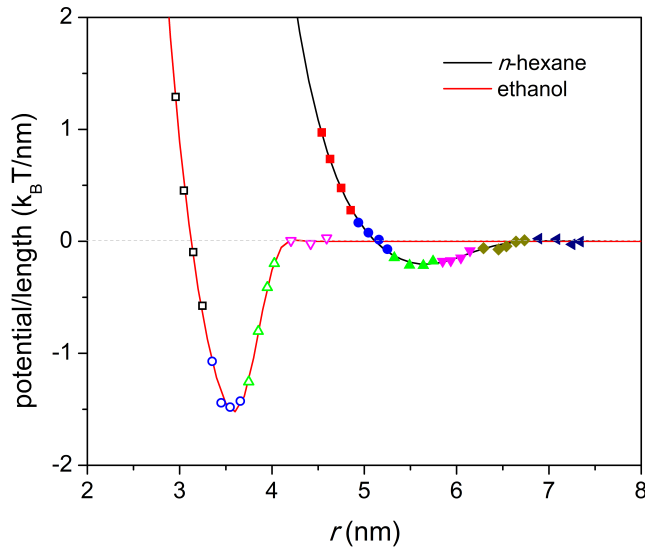


Figure 3: Potentials of mean force per unit length (PMF) for wire-wire interaction in *n*-hexane and ethanol (data points—converted MD results with colors identifying various r_s , solid lines—fitted PMFs). Fitting parameters can be found in table 2. Note that $k_B T$ in this graph refers to the thermal energy at room temperature and not to $T = 330$ K used in the simulations.

combined $F(r)$ with the following function:

$$W(r) = V_{\text{rep}} \exp\left(-\frac{r}{\rho_{\text{rep}}}\right) - V_{\text{adh}} \left[1 - \text{erf}\left(\frac{r - r_{\text{adh}}}{\rho_{\text{adh}}}\right)\right], \quad (4)$$

where V , ρ , and r_{adh} are fitting parameters. This potential outperformed all other tested two-body potentials. For example, fits to the data using Eq. 4 resulted in lower standard deviations (27 % and 68 % lower in the cases of *n*-hexane and ethanol, respectively) compared to Mie potentials having the form $V(r) = \epsilon[n(\zeta/r)^m - m(\zeta/r)^n]/(m-n)$, where ϵ (the binding energy), ζ (the equilibrium distance), m and n are adjustable parameters.

Fig. 3 shows the PMFs for both solvents, *n*-hexane and ethanol. The NWs immersed in good solvents reveal a distinctly smaller minimum in $W(r)$ at a larger separation r_{min} compared to the poor solvent. The observed trends reflect those seen in reported data and a small set of new experiments, which was conducted to accompany the simulations and to assess the effect of solvents on interwire distance. In the experiments, the wires were carefully purified to exclude effects of excess oleylamine (OA), which is known to strongly affect spacing. Care was taken not to desorb too much OA, which would reduce the ligand shell density and could also effect the spacing. The distances between the wires were then reconstructed in different solvents using small-angle X-ray scattering (SAXS), radial integration, and fitting.

The simulations find ≤ 15 % smaller spacings between NWs in ethanol than the experiments, specifically, 3.55 nm versus 4.10 nm (see Fig. S1). For *n*-hexane, the spacings even turn out almost identically, i.e. 5.51 nm (simulations) and 5.50 nm (experiments). Discrepancies of order 20 % between simulations and experiments are expected most notably because of differences in the grafting densities. The value of 3.8 ligands/nm² used in the simulations falls within the range of experimental estimates (2 to 8 ligands/nm²),^{24,29,30} which suffer from a large degree of currently unavoidable uncertainty.³⁰ This uncertainty cannot be eliminated experimentally because there is no technique available that would provide the ligand

density of individual wires, and because it is unknown how broad the standard deviation of the density over many wires is. Inaccuracies in the simulations result from the simplified treatment of the Au-N bond between the ligand and the core, and, more generally, from small imprecisions in the used potential energy surface, which is scarcely ever exact. Thus, the extremely good agreement for the NW spacing in *n*-hexane is certainly fortuitous to some degree. We would yet argue that the simulations certainly reproduce the trends correctly for the right reason. This does not only include the location of the (free-) energy minima but also their depths. Spheres with a radius R similar to that of the simulated wires agglomerate in the poor solvent ethanol, while they are stable against agglomeration in *n*-hexane.¹⁷ This is consistent with our values for the depth of the free-energy line density of wires with $R \approx 1.6$ nm, which is $1.52 k_B T/\text{nm}$ for ethanol but only $0.20 k_B T/\text{nm}$ for *n*-hexane.

3.2 Molecular morphology

In order to understand the underlying molecular origins of bundling in both solvents, we studied the morphology of both ligand and solvent molecules. To this end, the systems were simulated at their equilibrium interwire distance over a period of 20 ns.

Snapshots of the MD simulations are shown in Fig. 4a+b. They indicate that the ligand shells strongly interdigitate in the case of ethanol but barely touch in *n*-hexane. This can be seen more clearly in the quantitative contour plots in Fig. 4c-f, which show the density of ligand (c,d) and solvent (e,f) atoms projected onto the xy -plane.

The polar solvent ethanol is completely expelled from the interface between both nanowires (Fig. 4e), and the interdigitated ligands within the interface exhibit the largest atom densities throughout the simulations (see Fig. 4c and Fig. S2 in the SI). The 2D radius of gyration (R_g) of the ligands is shorter in ethanol ($R_g = 4.69 \text{ \AA}$) than in the good solvent *n*-hexane ($R_g = 4.93 \text{ \AA}$). Note that the surface-to-surface separation of the nanowires is only about 1.9 nm, approximately the length of one oleylamine ligand molecule. Bundling in ethanol is driven by minimizing the interfacial area between polar and apolar phases.

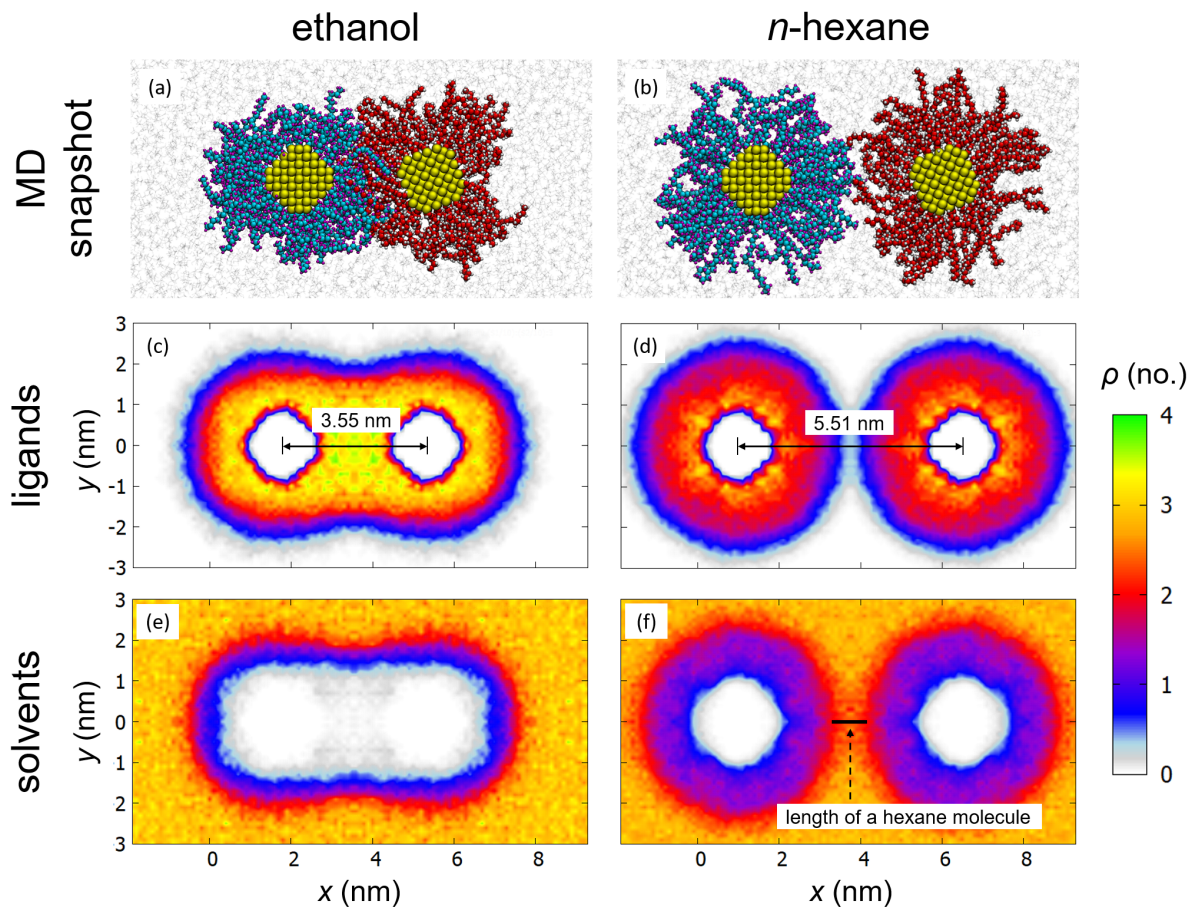


Figure 4: Representative snapshots of the MD simulations in (a) ethanol and (b) *n*-hexane and projected atom number densities of (c,d) the ligands and (e,f) the solvent molecules. ρ is with respect to each bin with dimensions of $0.1 \times 0.1 \times l_z \text{ nm}^3$.

In the apolar solvent *n*-hexane, Fig. 4d,f reveal that the ligand shells of two neighboring nanowires do not touch. There is enough space in between the ligand shells for at least one layer of *n*-hexane molecules. Furthermore, solvent molecules penetrate the shell (Fig. 4f), which is in line with the notion that *n*-hexane is a good solvent for oleylamine grafted nanowires. For the case of *n*-hexane, the formation of bundles cannot be explained by “classic” colloidal interaction potentials such as the interplay between attractive van der Waals forces and repulsive steric forces.^{31–33} The increased equilibrium separation between the wires cannot be due to swelling by the good solvent, either. Replacing ethanol with *n*-hexane leads to a swelling of the ligand shells by less than 2 Å, which certainly does not explain the increase of almost 1.5 nm that we observe.

To elucidate the role of *n*-hexane molecules in between two nanowires, we studied their degree of order with Herman’s orientation function ψ_i , defined as $\psi_i = \frac{3}{2} \langle (\hat{n}_{EE}^i \cdot \hat{n}_{COM}^i)^2 - \frac{1}{3} \rangle$, where \hat{n}_{EE} is a unit vector from one end-carbon to the other end-carbon of a solvent molecule, and \hat{n}_{COM} is a unit vector from the center of the closer nanowire to the center of that molecule. This defines ψ ranging from -0.5 to 1, where $\psi = -0.5$ when the director \hat{n}_{EE} is perpendicular to \hat{n}_{COM} and $\psi = 1$ when $\hat{n}_{EE} \parallel \hat{n}_{COM}$. Random orientation as it occurs in the liquid phase leads to $\psi = 0$. However, other distributions may also lead to $\psi = 0$.

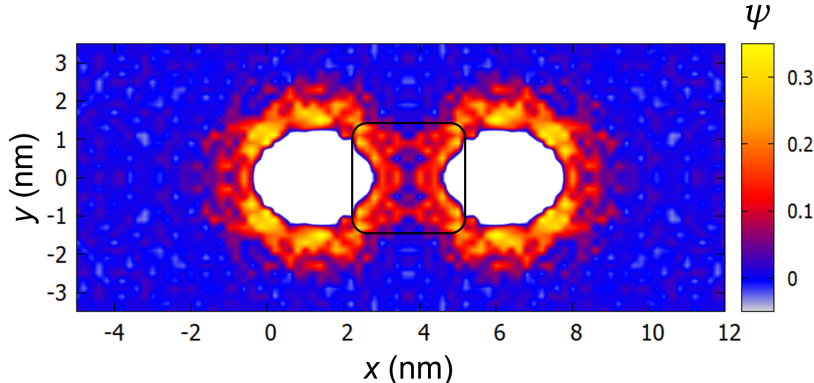


Figure 5: Contour plot of the orientational order parameter ψ evaluated for *n*-hexane molecules and projected onto the *xy*-plane. A value of ψ exceeding zero indicates a preferential orientation perpendicular to the nearest wire surface, while negative values indicate a preferential parallel orientation.

Fig. 5 shows ψ obtained for *n*-hexane by averaging over the *z*-direction and a period of 20 ns. In the bulk solvent, *n*-hexane molecules are randomly distributed. Within the ligand shell and in its direct proximity, $\psi_i > 0$, indicating that *n*-hexane molecules have a tendency to align their backbone normal to the Au surface. Oriented solvent molecules “bridge” the space in between the nanowires that is highlighted by the black frame in Fig. 5.

Ordering of the solvent is associated with a decrease in entropy. This decrease in entropy must be the reason for bundle formation. Nanowires bundle in *n*-hexane because they can “share” ordered solvent. If the nanowires remained dispersed, solvent would have to be ordered around each nanowire and the decrease in entropy would scale linearly with the length and number of nanowires. By forming bundles, solvent in between the nanowires only needs to be ordered once, and the system can keep a larger fraction of solvent in an disordered, high-entropy state.

4 Conclusions

It is rare to find that local solvent ordering induces the agglomeration of colloidal particles. In classical theory, the “combinatorial” (purely entropic) contribution to the total free energy of solvent and ligand molecules in a dispersion is assumed to always increase with decreasing particle separation, because removing solvent from stabilizing shells increases entropy. This is usually the dominating stabilizing term for nonaqueous dispersions.³⁴

The line contact between the very thin wires used here makes it possible for solvent molecules to “bridge” two ligand shells along many micrometers. The free energy gain associated with the entropic bundling mechanism is on the order of $0.2 k_B T/\text{nm}$. This bridging over a line contact is geometrically impossible for small spheres. A similar mechanism may exist in planar contacts, although the constraints of packing may reduce the order in a hypothetical single solvent layer between two planes, depending on the ligand structure. It would be interesting to explore this possibility in apolar dispersions of 2D materials such as

nanoplatelets.^{35,36}

The existence of this bundling mechanism has several practical implications. Local order is sensitive to the exact molecular structure of the solvent, and one would expect large differences in colloidal stability for solvents that have similar bulk properties but different structures such as *n*-hexane and cyclohexane. This should make it possible to precisely tune the spacing between wires and thus control their coupling, for example to control the fluorescence of semiconductor nanowires,^{37,38} tune charge carrier tunneling between metal nanowires,³⁹ or modulate the mechanical properties of fibres made from nanowires.¹²

If bundling is undesirable, it will be useful to perturb the order of the solvent layer and suppress entropic bundling. Recent results on the stability of spherical nanoparticles suggest that this may be possible by using suitable ligand molecules.⁴⁰

Acknowledgement

The authors gratefully acknowledge the Gauss Centre for Supercomputing e.V. (www.gauss-centre.eu) for funding this project by providing computing time through the John von Neumann Institute for Computing (NIC) on the GCS Supercomputer JUQUEEN at Jülich Supercomputing Center (JSC). HG thanks the Alexander von Humboldt Foundation for the research fellowship.

SB thanks the Foundation of German Business for his PhD scholarship. The authors would like to thank Lukas F. Engel for help with the synthesis of gold nanowires, Anna Zimmermann and David Doblás Jiménez for support in acquiring SAXS measurements, and Lola González-García for recording TEM micrographs. Vikrant Naik is acknowledged for fruitful discussions.

References

- (1) Halder, A.; Ravishankar, N. Advanced Materials **2007**, 19, 1854–1858.
- (2) Huo, Z.; Tsung, C.-k.; Huang, W.; Zhang, X.; Yang, P. Nano Letters **2008**, 8, 2041–2044.
- (3) Wang, C.; Hu, Y.; Lieber, C. M.; Sun, S. Journal of the American Chemical Society **2008**, 130, 8902–8903.
- (4) Saitoh, M.; Kashiwagi, Y.; Chigane, M. Soft Matter **2017**, 13, 3927–3935.
- (5) Lu, X.; Yavuz, M. S.; Tuan, H.-y.; Korgel, B. A.; Xia, Y. Journal of the American Chemical Society **2008**, 130, 8900–8901.
- (6) Feng, H.; Yang, Y.; You, Y.; Li, G.; Guo, J.; Yu, T.; Shen, Z.; Wu, T.; Xing, B. Chemical Communications **2009**, 0, 1984–1986.
- (7) Loubat, A.; Impéror-Clerc, M.; Pansu, B.; Meneau, F.; Raquet, B.; Viau, G.; Lacroix, L.-M. Langmuir **2014**, 30, 4005–4012.
- (8) Sánchez-Iglesias, A.; Rivas-Murias, B.; Grzelczak, M.; Pérez-Juste, J.; Liz-Marzán, L. M.; Rivadulla, F.; Correa-Duarte, M. A. Nano Letters **2012**, 12, 6066–6070, PMID: 23167827.
- (9) Maurer, J. H. M.; González-García, L.; Reiser, B.; Kanelidis, I.; Kraus, T. Nano Letters **2016**, 16, 2921–2925.
- (10) Maurer, J. H. M.; González-García, L.; Backes, I. K.; Reiser, B.; Schlossberg, S. M.; Kraus, T. Advanced Materials Technologies **2017**, 2, 1700034.
- (11) Gong, S.; Lai, D. T.; Wang, Y.; Yap, L. W.; Si, K. J.; Shi, Q.; Jason, N. N.; Sridhar, T.; Uddin, H.; Cheng, W. ACS Applied Materials & Interfaces **2015**, 7, 19700–19708.

- (12) Reiser, B.; Gerstner, D.; Gonzalez-Garcia, L.; Maurer, J. H. M.; Kanelidis, I.; Kraus, T. ACS Nano **2017**, 11, 4934–4942.
- (13) Reiser, B.; Gerstner, D.; Gonzalez-Garcia, L.; Maurer, J. H. M.; Kanelidis, I.; Kraus, T. Physical Chemistry Chemical Physics **2016**, 18, 27165–27169.
- (14) Nouh, E. S. A.; Baquero, E. A.; Lacroix, L.-M.; Delpech, F.; Poteau, R.; Viau, G. Langmuir **2017**, 33, 5456–5463.
- (15) Wang, F.; He, C.; Han, M. Y.; Wu, J. H.; Xu, G. Q. Chemical Communications **2012**, 48, 6136–6138.
- (16) Sánchez-Iglesias, A.; Grzelczak, M.; Pérez-Juste, J.; Liz-Marzán, L. M. Angewandte Chemie - International Edition **2010**, 49, 9985–9989.
- (17) Lau, C. Y.; Duan, H.; Wang, F.; He, C. B.; Low, H. Y.; Yang, J. K. W. Langmuir **2011**, 27, 3355–3360.
- (18) Peng, S.; Lee, Y.; Wang, C.; Yin, H.; Dai, S.; Sun, S. Nano Research **2008**, 1, 229–234.
- (19) Teraoka, I. Polymer Solutions; John Wiley & Sons, Inc.: New York, USA, 2002.
- (20) Mukherji, D.; Marques, C. M.; Kremer, K. Nature Communications **2014**, 5, 4882.
- (21) de Beer, S.; Kutnyanszky, E.; Schön, P. M.; Vancso, G. J.; Müser, M. H. Nature Communications **2014**, 5, 3781.
- (22) Fraser, B.; Denniston, C.; Müser, M. H. Journal of Polymer Science Part B: Polymer Physics **2005**, 43, 970–982.
- (23) Khanal, B. P.; Zubarev, E. R. Angewandte Chemie International Edition **2007**, 46, 2195–2198.
- (24) Sebbby, K. B.; Mansfield, E. Analytical and Bioanalytical Chemistry **2015**, 407, 2913–2922.

- (25) Quek, S. Y.; Venkataraman, L.; Choi, H. J.; Louie, S. G.; Hybertsen, M. S.; Neaton, J. B. Nano Letters **2007**, 7, 3477–3482.
- (26) Jorgensen, W. L.; Maxwell, D. S.; Tirado-Rives, J. Journal of the American Chemical Society **1996**, 118, 11225–11236.
- (27) Plimpton, S. Journal of Computational Physics **1995**, 117, 1–19.
- (28) O’Hagan, A.; Leonard, T. Biometrika **1976**, 63, 201–203.
- (29) Huber, S. E.; Warakulwit, C.; Limtrakul, J.; Tsukuda, T.; Probst, M. Nanoscale **2012**, 4, 585–590.
- (30) Smith, A. M.; Johnston, K. A.; Crawford, S. E.; Marbella, L. E.; Millstone, J. E. The Analyst **2017**, 142, 11–29.
- (31) Cölfen, H.; Mann, S. Angewandte Chemie International Edition **2003**, 42, 2350–2365.
- (32) Ozin, G. A.; Hou, K.; Lotsch, B. V.; Cademartiri, L.; Puzzo, D. P.; Scotognella, F.; Ghadimi, A.; Thomson, J. Materials Today **2009**, 12, 12–23.
- (33) Bishop, K. J. M.; Wilmer, C. E.; Soh, S.; Grzybowski, B. A. Small **2009**, 5, 1600–1630.
- (34) Napper, D. H. Polymeric stabilization of colloidal dispersions; Academic Press Inc.: London, New York, 1983.
- (35) Abécassis, B.; Testard, F.; Spalla, O.; Barboux, P. Nano Letters **2007**, 7, 1723–1727.
- (36) Jana, S.; De Frutos, M.; Davidson, P.; Abécassis, B. Science Advances **2017**, 3.
- (37) Fujiwara, M.; Toubaru, K.; Noda, T.; Zhao, H. Q.; Takeuchi, S. Nano Letters **2011**, 11, 4362–4365.
- (38) He, J.; Li, J.; Xia, J.; Tian, L.; Jin, B.; Zhou, S.; Sun, M.; Meng, X. Advanced Materials Interfaces **2019**, 6, 1–9.

- (39) Loubat, A.; Escoffier, W.; Lacroix, L.-M.; Viau, G.; Tan, R.; Carrey, J.; Warot-Fonrose, B.; Raquet, B. Nano Research **2013**, 6, 644–651.
- (40) Monego, D.; Kister, T.; Kirkwood, N.; Mulvaney, P.; Widmer-Cooper, A.; Kraus, T. Langmuir **2018**, 34, 12982–12989.